Schietroma et al., https://doi.org/10.1083/jcb.201612030

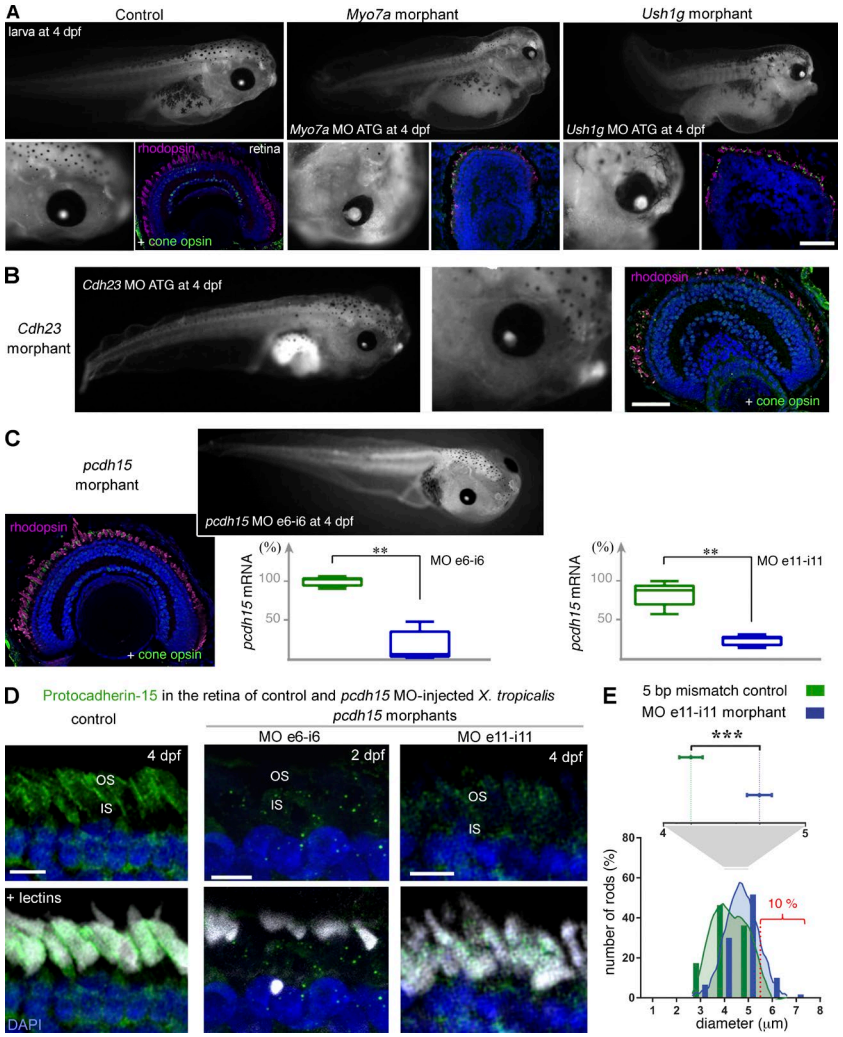

Figure S1. **Effect of antisense morpholino oligonucleotides against USH1 gene transcripts in *X. tropicalis* larvae.** (A) Morpholino (MO) antisense oligonucleotides designed to block the translation of *Xenopus myo7a*, *Ush1c*, or *Ush1g* did not cause retina-specific abnormalities in larvae when low doses of these MOs were microinjected in *X. tropicalis* zygotes; conversely, higher doses often led to premature growth arrest and substantial developmental defects in the survivors, which precluded analysis of a specific retinal phenotype. Examples of *myo7a* and *Ush1g* morphants at 4 dpf are shown, displaying shorter and curved bodies, microphthalmia, and incomplete closure of the choroidal fissure. Cryosections of the eyes stained with DAPI (blue-stained nuclei) and antibodies against rhodopsin and cone opsin reveal defective retinal lamination as well as grossly disorganized photoreceptor outer segments. (B) Knockdown of *cdh23* using splice site and translation blocking antisense MOs. Severe and generalized developmental defects were occasionally observed, complicating the analysis of retina-specific abnormal phenotypes. Nonetheless, *cdh23* morphant retinas at 4 dpf display near-normal laminated organization, with differentiated rod and cone photoreceptors. (C) *Pcdh15* morphants did not present with gross developmental defects, and the retinal layers were well preserved. In the graphs, densitometric quantification of correctly spliced *pcdh15* transcripts in MO e6-i6 and MO e11-i11 morphants at 4 dpf were normalized to the amount of *gapdh* transcripts and are expressed as the percentage of noninjected controls: MO e6-i6 mismatch: 95.8–104.2% (95% CI) versus MO e6-i6: 5.9–25.8% (95% CI; **); MO e11-i11 mismatch 67.7–99.4% (95% CI) versus 19.4–29.6% (95% CI; **), $n = 6–8$. Representative gels showing semiquantitative RT-PCR analysis of amplicons containing exon 6 and exon 11 are shown in Fig. 1 B. (D) Immunostainings of retinal cryosections with HPEx antibodies at 2 dpf show protocadherin-15 labeling around the outer segments (OS), just emerging from the inner segment (IS). OS are counterstained with the WGA and peanut agglutinin lectins. Staining is greatly reduced in retinas of age-matched, morphant larvae microinjected with MO e6-i6 (the staining in MO e6-i6 morphants at 4 dpf is shown in Fig. 1 C). Likewise, the protocadherin-15 staining is reduced, although not abolished, in 4 dpf retinas of morphant larvae microinjected with MO e11-e11. (E) The basal diameter of rhodopsin-stained photoreceptors in MO e11-i11 *pcdh15* morphants was found to have 10% of the rods with a diameter larger than that of control photoreceptors (unpaired *t* test, ***, $P < 0.001$; the cutoff was defined as two SDs greater than the mean; 6 of 60, corresponding to the nonoverlapping region of the morphant and control distributions). Bars: (A–C) 50 µm; (D) 5 µm.

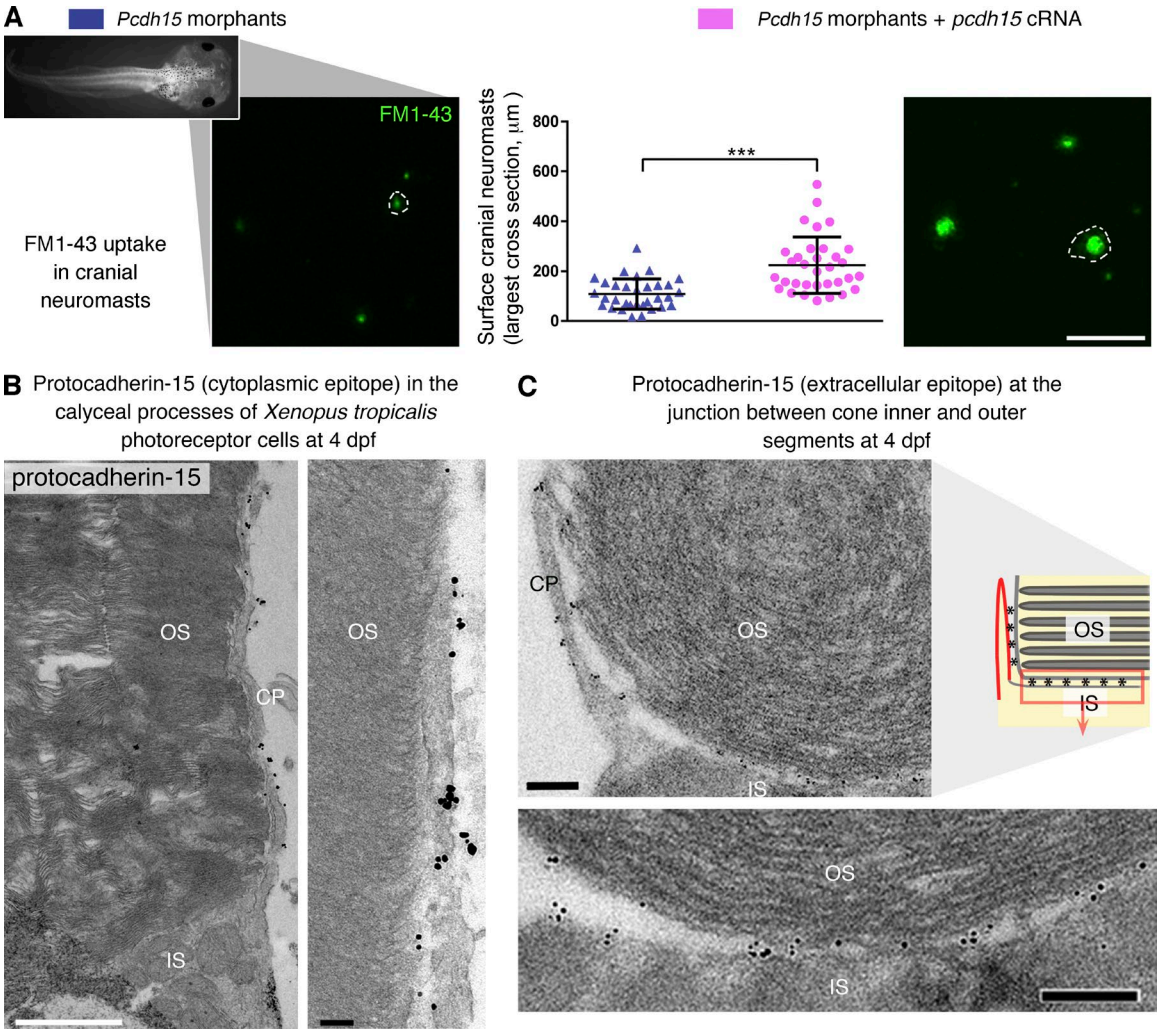

Figure S2. **Effect of the coinjection of MO e6-i6 and cRNAs coding for protocadherin-15 CD1 and CD3 isoforms on the uptake of FM1-43 fluorescent dye by cranial neuromast hair cells in *X. tropicalis larvae* and distribution of protocadherin-15 in the retinal photoreceptor cells.** (A) The effect of the coinjection of MO e6-i6 and cRNA coding for protocadherin-15 CD1 and CD3 isoforms was assessed by measuring the FM1-43 uptake by cranial neuromast hair cells in 3 dpf larvae. The MOs (25 bp long) could not interfere with the cRNA of *pcdh15* because only 5–6 bp correspond to exonic regions of the *pcdh15* transcripts (see Materials and methods). In z stacks obtained by spinning-disk live imaging, we measured the cross section of cranial neuromasts labeled with FM1-43 (outlined). Measured areas were significantly larger in morphants derived from embryos coinjected with the cRNAs compared with those derived from embryos injected with the sole MO e6-i6 (224.5 ± 19.7 mm^2 in morphants + cRNAs, n = 33 versus 120.6 ± 15.5 mm^2 in morphants, n = 33, mean ± SEM, unpaired t test, ***, P = 0.0001). (B) Representative images of pre-embedding immunogold localization of protocadherin-15 at the photoreceptor calyceal processes (CP), with an antibody directed against a cytoplasmic epitope adjacent to the transmembrane domain (XPJM, see Fig. 1 A). OS, outer segment. (C) A subset of cones display immunogold labeling for protocadherin-15 (HPEx) at the inner segment (IS)–OS junction. Bars: (A) 20 µm; (B, left image) 1 µm; (B, other panels) 100 nm; (C) 200 nm.

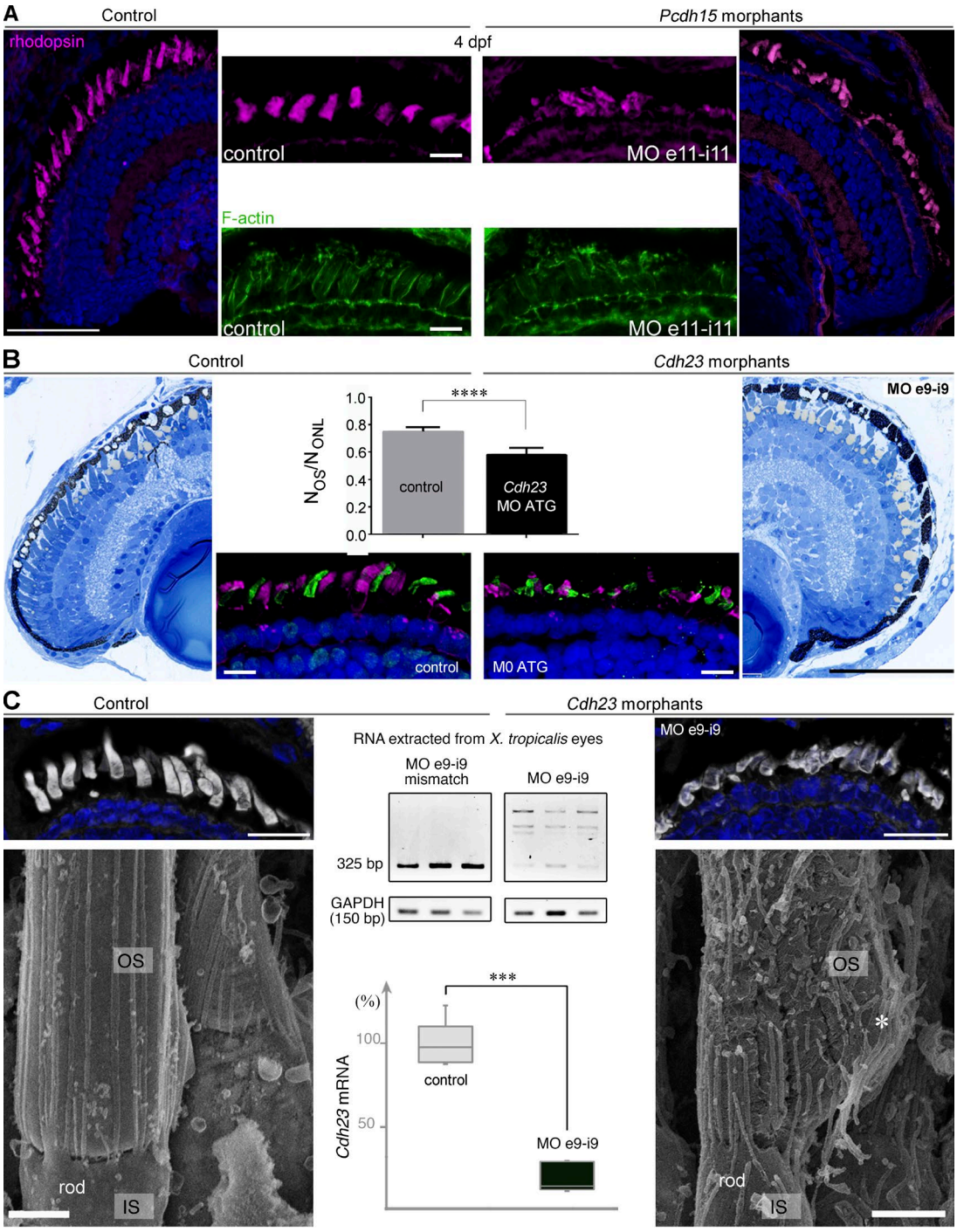

Figure S3. **Alterations of photoreceptor outer segments in *pcdh15* and *cdh23* morphants.** (A) Morpholinos targeting the splice donor site at the 3′ end of *pcdh15* exon 11 (MO e11-i11) cause abnormal photoreceptor outer segments (OS) and disorganization of the actin cytoskeleton in 4 dpf morphant larvae. (B) Semithin sections and cryosections of *cdh23* morphant retinas stained with opsins reveal proper organization of the retinal layers, but the subretinal space is disorganized in morphant retinas (examples of data obtained with splice-interfering morpholinos directed against the splice donor site at the 3′ end of *cdh23* exon 9 [MO e9-i9] and translation-blocking morpholinos [MO ATG] are shown). The ratio of OS to cell nuclei numbers (N_{OS}/N_{ONL}) is significantly reduced in *cdh23* morphant retinas: 0.60 ± 0.02 in morphants (mean ± SEM, $n = 5$), versus 0.75 ± 0.01 in controls; unpaired *t* test, ****, P = 0.0005 ($n = 4$). (C, middle) Representative gel showing semiquantitative RT-PCR analysis of amplicons containing *cdh23* exon 9 and the effect of MO e9-i9 on splicing; in the graph, densitometric quantification of correctly spliced *cdh23* transcripts in MO e9-i9 morphants at 4 dpf, normalized to the amount of *gapdh* transcripts (control/MO e9-i9 mismatch: 82.7–117.3% (95% CI) versus MO e9-i9: 10.4–37.6% (95% CI; ***); $n = 3–5$. In the lateral panels, the photoreceptor OS of *cdh23* morphant larvae stained with the fluorescent WGA and peanut agglutinin lectins are misshapen and deformed. Scanning electron microscopy analysis reveals that rod outer segments have basal enlargements (asterisk), and cone outer segments are curved and misaligned. Bars: (A and B, lateral) 50 µm; (A and B, middle) 10 µm; (C, top) 20 µm; (C, bottom) 2 µm.

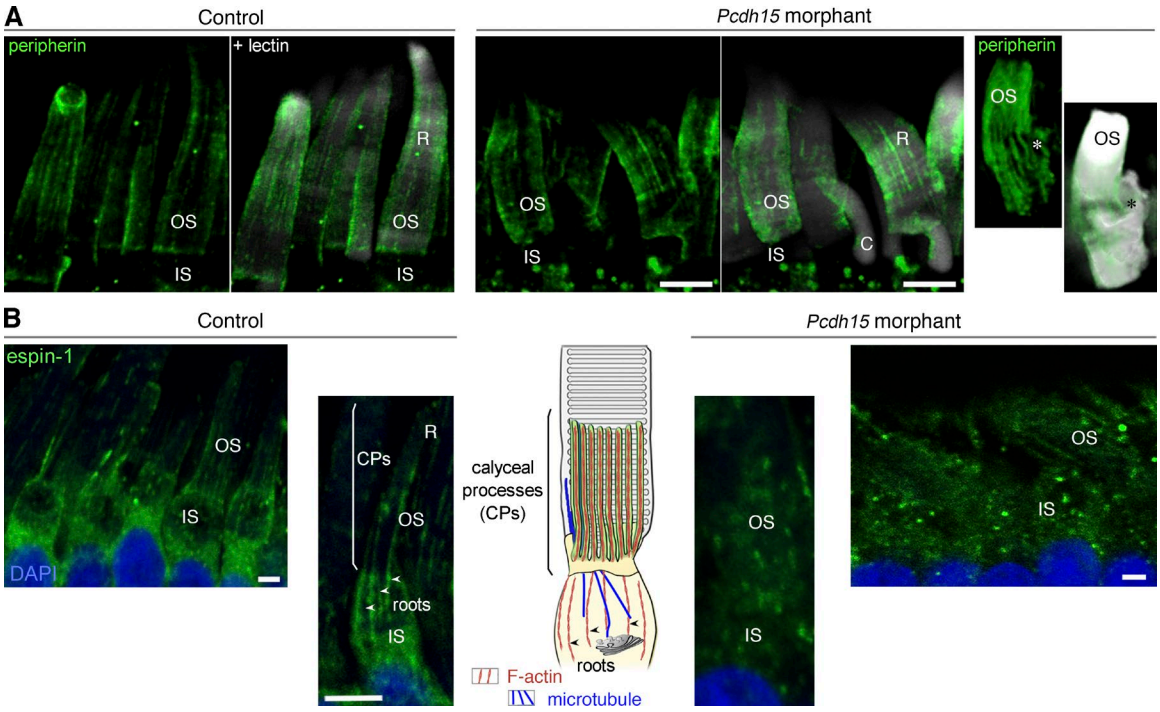

Figure S4. **Normal distribution of peripherin and espin in photoreceptor cells of p*cdh15* morphant larvae.** (A) *Pcdh15* knockdown does not affect the localization of peripherin/RDS. In the control and morphant rod photoreceptor cells, peripherin/RDS staining has the characteristic, striated pattern, corresponding to the incisures of the rod outer segments. 3D rendering of a morphant rod stained for peripherin/RDS and counterstained with the WGA lectin suggests that the outer segment (OS) basal enlargements retain peripherin staining (asterisks). (B) In the morphant photoreceptors, espin staining is reduced in calyceal processes (CPs) and their F-actin roots. C, cone; IS, inner segment, R, rod. Bars: (A) 5 µm; (B) 2 µm.

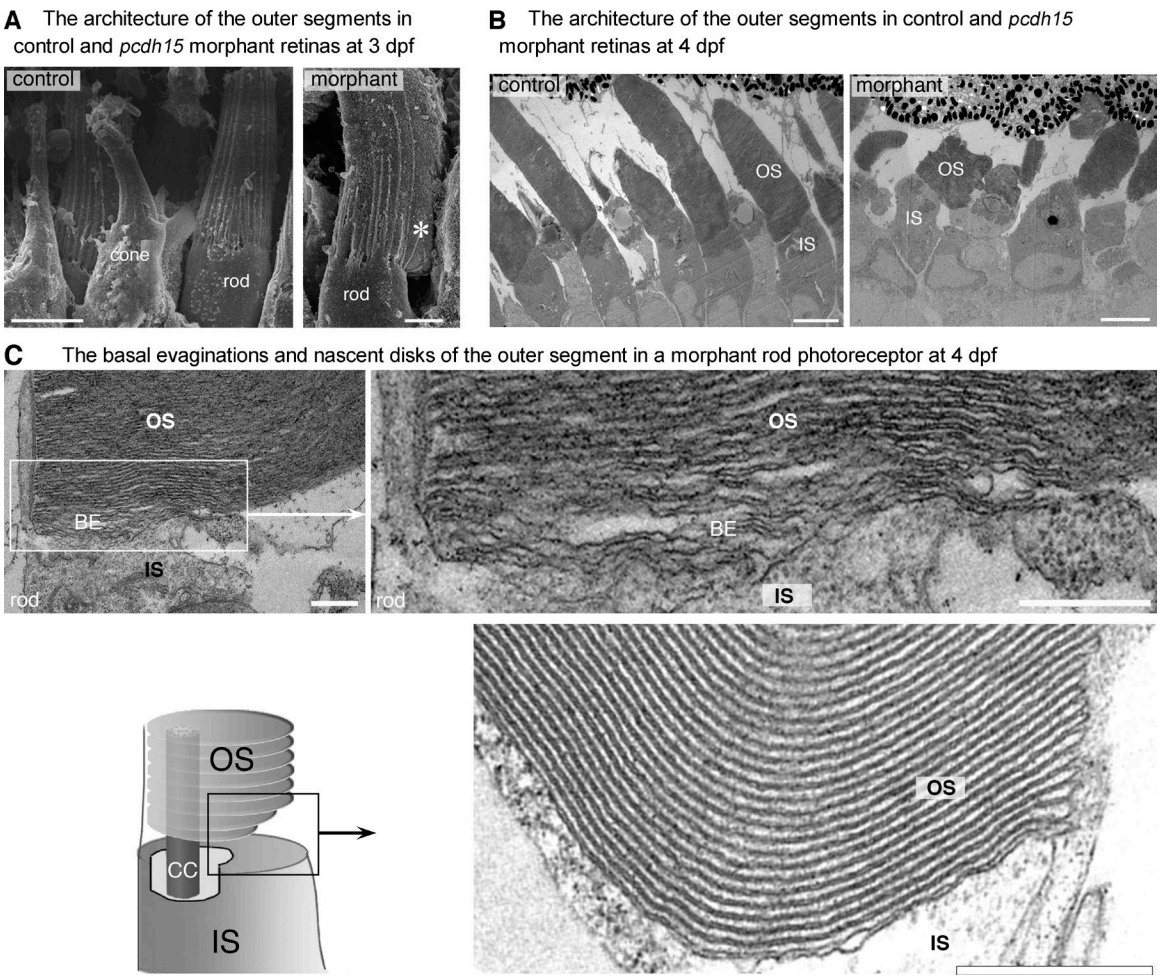

Figure S5. **The ultrastructure of photoreceptor outer segments in 3-dpf and 4-dpf *pcdh15* morphant larvae.** (A) Scanning electron microscopy analysis shows that, at 3 dpf, rod photoreceptors are well developed, although they still have conical shapes. In control retinas, the base of the rod outer segments (OS) and the apex of the inner segment (IS) are congruent, whereas morphant rods display an enlarged OS base (asterisk). (B) Transmission electron micrographs of thin sections at 4 dpf reveal mostly parallel OS profiles, with conical or cylindrical shapes, in controls. In morphants, the OS profiles vary more in shape and are fragmented, which is consistent with sections cut through bent and misshapen OS. (C) In rod OS with an abnormally enlarged base, it is possible to distinguish basal evaginations; they are open to the extracellular space and are organized in a staircase pattern toward the edge of the IS. Bars: (A) 2 µm; (B) 5 µm; (C) 500 nm.

Provided online is the Script.txt file, which includes the code used in Matlab (MathWorks) for analysis of ERG recordings.